www.lajss.org
Latin American Journal of Solids and Structures 1 (2004)319–339

Material testing at high strain rate using the split Hopkinson pressure bar

S.T. Marais, R.B. Tait, T.J. Cloete and G.N. Nurick*

Blast, Impact and Survivability Research Unit (BISRU)
Department of Mechanical Engineering, University of Cape Town
Private Bag Rondebosch, 7701, Cape Town

Abstract

This paper reports on a particularly accurate and precise physical and experimental data capture and data processing system for high strain rate testing using the split Hopkinson pressure bar. The data processing incorporated the first four Pochammer-Chree modes and proved to be suitable for the tests that were carried out. To vindicate the design of the facility, two materials were tested, namely mild steel and copper, in both the as-received and annealed conditions. The actual test data, once appropriately processed was compared with both the Johnson-Cook (JC) and Cowper-Symonds (CS) high strain rate materials models, as well as with other published data. The correlation with previously published constants for the JC and CS models was not particularly good, due to perceived differences in the stress levels and prior work hardening, heat treatment condition and microstructure of these earlier tests, as these variables affect the constitutive equation constants. Using other published data, however, the correlation was improved, suggesting there is scope for modification and improvement of these constitutive equation parameters in the classic approaches.

Keywords: split Hopkinson bar, dynamic material response, material characterisation

1 Introduction

As a result of increasing demand to improve analysis of fast manufacturing techniques as well as safety in structures, it is necessary to determine accurate and reliable material properties at high strain rates. Conventional screw-driven or servo-hydraulic methods of testing materials at high strain rates are not entirely adequate as the strain rates are limited and also there are oscillations and stress waves set-up within the testing apparatus at high speeds. These oscillations and stress waves impair the transducer load cell reading, thus making the data obtained more complex to interpret reliably. These limitations were overcome with the development of the Hopkinson pressure bar (SHPB) [9], subsequently extended by Davies [5] and Kolsky [13]. Even with such a SHPB facility, data instrumentation, data capture and processing is of critical importance if

* Corresponding author E-mail: gnurick@ebe.uct.ac.za Received 02 July 2004; In revised form 30 July 2004

reliable material data is to be obtained. This paper aims specifically at addressing this accuracy and reliability issue. The paper first covers the development of data capturing and processing as well as discussing the relevant theory for the SHPB. Two numerical models, the Cowper-Symonds and Johnson-Cook constitutive equations are discussed as these were used as a reference for test results. The full experimental operation is discussed together with experimental results and findings and concluding with future capabilities of the system.

1.1 Review of the Development of Data Capturing and Processing

The central challenge in SHPB operation and research has always been to obtain reliable stress wave measurements. This section discusses the development of the data capturing and processing of the signals from the SHPB.

The initial work by Davies (1948) [5] and Kolsky (1949) [13] used cylindrical condenser microphones, and capacitive sensors mounted on the bars to measure the stress wave propagation as conventional resistive strain gauges had not yet been developed. The signal was amplified approximately 3000 times using valve amplifiers, which limited the frequency response, and fed into a cathode ray oscilloscope. Along with the signal from the amplifier, a sinusoidal wave was fed into the second channel, to provide a reference timing trace. When the pulse was applied to the bar, by either explosive loading or by projectile, an inertial switch mounted on the bar would trigger a camera to photograph the trace generated by the oscilloscope. The film was developed and photograph enlarged so that the trace could be used to generated a stress-strain curve for the material tested.

The analysis of the results from the split Hopkinson pressure bar was based on the assumption that one dimensional wave theory was adequate. To improve the accuracy of the analysis, dispersion of the wave had to be considered. Dispersion of the pulse in this case refers to the fact that the higher frequency components of the pulse travel slower in the bar than the low frequency components. This meant that the pulse "broke-up" or dispersed at it moved down the bar. This is overcome by correcting the signal for dispersion using the so-called Pochhammer-Chree curves as investigated by Bancroft [4]. These refer to the solution of the equation of motion for wave propagation in an infinitely long cylindrical bar. The generation and use of the Pochhammer-Chree curves is discussed in more detail in Section 2.2 and 2.3.

To illustrate the break-up of the pulse due to the dispersion, a trapezoidal shaped pulse was assumed to be initiated at the end of the pressure bar. As the pulse moved down the bar, dispersion occurs according to the first Pochhammer-Chree mode. It can be seen in Figure 1 that the low frequency components of the pulse stay within the main body, whereas the high frequency components form a "tail" at the rear of the pulse. What is also evident, as a result of the separation of the frequencies, is the formation of oscillations on the main body of the pulse. These oscillations result in oscillations on the stress-strain curve, which distort the true stress-strain state of the specimen.

Davies [5] applied the numerical results calculated from the Pochhammer-Chree equation to

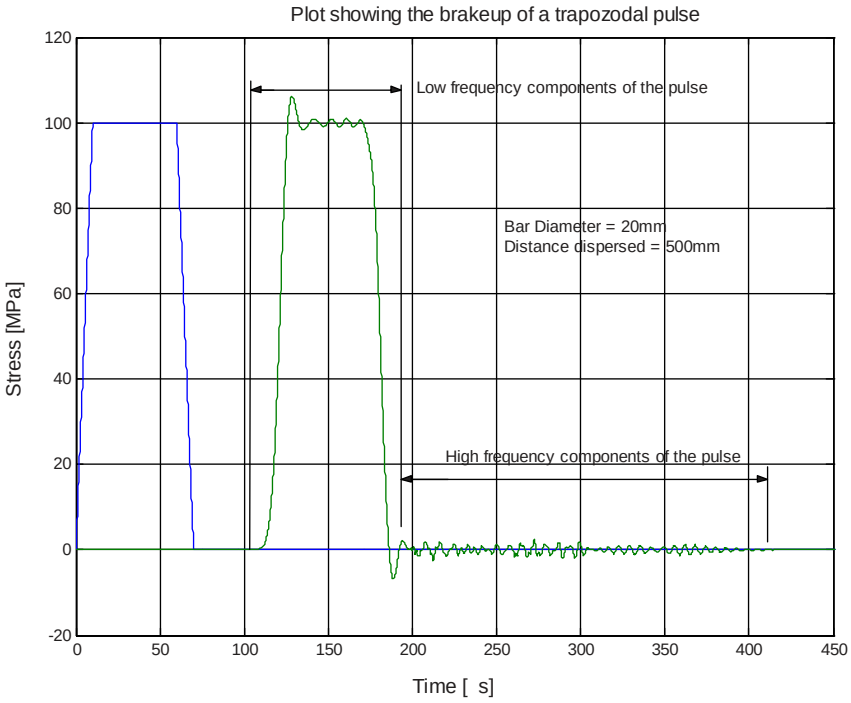

Figure 1: Plot showing the break-up of a trapezoidal pulse due to dispersion.

determine the dispersion of a wave travelling in a bar. It was assumed that the pulse initiated at the end of the bar was trapezoidal and periodic, which could be expressed as a periodic wave by a Fourier series, allowing each component to travel with its phase velocity. Davies investigations showed that it was indeed possible to reconstruct a dispersive stress wave in a long cylindrical bar with prior knowledge of the diameter, Young's modulus, Poisson's ratio and the density of the bar. It was also shown that the wave propagation belonged predominantly to the first mode of vibration. This investigation method, at the time, was time consuming as all the calculations were performed manually. The number of Fourier terms was also limited which reduced the resolution of the corrected wave. Despite the computational limitations, however, it was possible to show that the wave propagation belonged to the first mode of vibration. In 1958 Hsieh and Kolsky [10] used a simpler method to confirm Davies work.

The development of the transistor and the improvement of computational equipment, made it possible to use Fast Fourier Transform (FFT) analysis techniques [18]. The FFT algorithm is used to transform the time domain data to the frequency domain. The final result is a complex expression of the magnitude and phase of each of the frequencies in the time domain. In 1978 Yew and Chen [21] captured a wave at two locations in a cylindrical aluminium rod simultaneously with an oscilloscope (by photographing the image) and a transient recorder. From the two readings at separate locations, together with the use of the FFT, Yew and Chen

were able experimentally, to plot the phase velocity. Acceptable correlation of the experimental phase velocity to the theoretical phase velocity (generated from the first Pochhammer-Chree dispersion curve) was obtained.

In 1983, Gorham [8] significantly reduced the oscillation on the generated stress-strain curve. The signal from the pressure bar was digitised, at a sample rate of 20MHz, and processed using the FFT algorithm on a HP9825 computer. Once the data was transformed he corrected the phase shift using tabulated data generated by Bancroft [4]. The Inverse Fast Fourier Transform (IFFT) was used to reconstruct the pulse to the time domain. This method was significantly different from the former methods as it did not use the assumption that the wave was trapezoidal and periodic. This meant that pulses that are not trapezoidal in shape, such as those generated from explosive detonation, could be corrected and processed.

Even though the method used by Gorham reduced the oscillation on the stress-strain curve it had not been removed completely. Lipshitz and Leber [16] investigated the source of these oscillations by noting the effect of small errors in the value used for the fundamental wave speed $C_0 = \sqrt{E/\rho}$ where E= Young's modulus and ρ = density of the bar. This was achieved by measuring the stress pulse in a bar at two locations and then shifting the reading of the first pulse to the second with the correction for dispersion. The method proposed by Gorham was used to correct for the dispersion, together with several values close to the correct fundamental wave speed to note the effect. It became apparent that an error of only 1% in the fundamental wave speed could significantly increase the oscillation on the stress-strain curve.

Up to this stage dispersion correction that had been employed, used the Pochhammer-Chree solution for the propagation of the wave, but this solution is only exact for bars of infinite length. Lee and Crawford [14] developed a method to measure the phase velocity of the stress pulse. The first version of the method used only one Hopkinson pressure bar and a sphere of high explosives was detonated at one end. The recorded signal was analysed with the rectangular-window Fourier transform technique to obtain the time-dependent Fourier coefficients from a measured signal. From this the phase velocities were obtained. These phase velocities took into account the time of arrival of each frequency, thus gaining a better representation of the actual phase velocity. The corrected phase velocities were used to correct for the dispersion of the pulse. The pulse measure was shifted to the loaded end of the bar and corrected for dispersion. The new trace of the pulse was compared to the method used by Gorham, and it was shown that the peak was far more clearly defined. There were also less oscillations ahead of the pulse indicating that the correct phase velocity had been used. This new method was more computationally costly, as 3000 data points were processed on an IBM 486 and the new method took 30 minutes to analyse, whereas the Gorham method took only 3 minutes.

The use of a rectangular-window in the Fourier transform meant that the higher frequencies were filtered out and any higher modes of vibration present were lost. Lee and Crawford [15] used the Gaussian-window Fourier transform technique to measure experimentally the Pochhammer-Chree dispersion curves. The same setup was used as in the previous experiment, but the signal was sampled by a high speed, high-resolution data recorder (sample rate of 10MHZ, sample size

of 10000 and 12 bit resolution). The transformed data showed the presence of four modes of vibration. The Pochhammer-Chree analytical solution and the transformed data were used to generate the new semi-empirical dispersion curve for the stress wave propagation in the bar. This new dispersion curve was used to shift the pulse to the loaded end of the bar. This method was compared to the method used by Gorham and it was noted that the rise time of the explosion was higher with the new method. The peak was also more defined and there were no oscillations preceding the pulse.

The work presented in this paper used the FFT along with the first four Pochhammer-Chree modes to correct for dispersion. The method used and relevant theory is discussed in the section that follows.

2 Summary of the Relevant Theory

2.1 One Dimensional Wave Propagation Theory

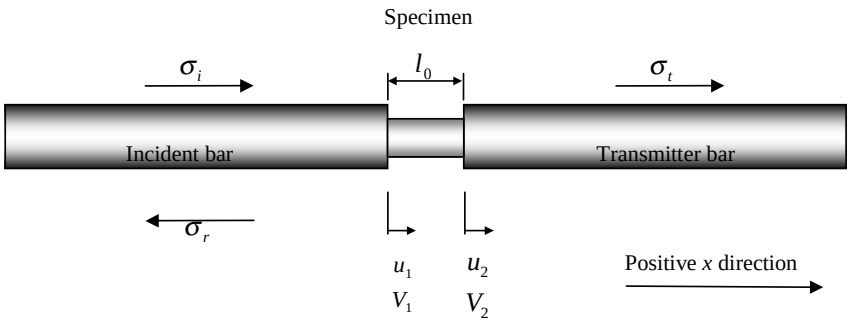

Figure 2: Schematic of the SHPB showing the stresses in the bar.

Wave propagation behaviour for elastic bars is well-understood and mathematically predictable [3]. From elementary wave theory the wave equation can be shown to be [6]:

$$\frac{\partial^2 u}{\partial x^2} = \frac{1}{C_0^2}\frac{\partial^2 u}{\partial t^2}$$

where $C_0 = \sqrt{\frac{E}{\rho}}$ is the fundamental longitudinal wave velocity, and u is the a displacement. From the wave equation the stress in the bar can be shown to be

$$\sigma = -\rho C_0 V$$

were ρ is the density of the bar and V the velocity of the particles of the bar subjected to the pulse.

The stress at the incident bar/specimen interface (σ_{S1}) is then

$$\sigma_{s1} = \frac{(\sigma_i - \sigma_r)A_{Bar}}{A_S\,(t)}$$

and the stress at the specimen/transmitter(σ_{S2})bar interface is

$$\sigma_{s2} = \frac{\sigma_t A_{Bar}}{A_S\,(t)}$$

were σ_i, σ_r and σ_t is the incident, reflected and transmitted stress in the bars. Assuming incompressible plasticity, then $A_0 l_0 = A_S l_S$, (where A_0 is the original cross-sectional area of the specimen, $A_S(t)$ is the instantaneous cross-sectional area the specimen, and A_{BAR} is the cross-sectional area of the bar).

Note that once the ringing up of the specimen is complete and the specimen has attained a stable stress state then $\sigma_{S1} = \sigma_{S2}$.

From the displacement of the two bars the true strain of the specimen is found. The true strain is

$$\varepsilon_{true} = \ln\left(\frac{l}{l_0}\right)$$

And by differentiating the strain with respect to time gives the strain rate in the specimen

$$\dot{\varepsilon} = \frac{v_1 - v_2}{l_S(t)}$$

2.2 Solution of the Equation of Motion

The solution to the equation of motion for the wave propagation in an infinitely long cylindrical bar was solved by Pochhammer (1876) and independently by Chree (1889). The solution relates the propagation velocity C_p to the wavelength A and is exact only for an infinitely long round bar, and is approximately correct for bars of finite length. An excellent summary of the Pochhammer-Chree solution has been given by Love [17], which Bancroft [4] has, for ease of computation, rewritten in the following form.

$$(x-1)^2\,\phi\,(ha) - (\beta x - 1)\,[x - \phi\,(ka)] = 0 \tag{1}$$

where
$x = (1+v)\left(\frac{C_p}{C_0}\right)^2$ C_p = Phase velocity
$\beta = \frac{1-2v}{1-v}$ C_0 = fundamental velocity $= \sqrt{\frac{E}{\rho}}$
$h = \gamma\sqrt{\beta x - 1}$ $\gamma = \frac{2\pi}{\Lambda}\Lambda =$
wavelength
$k = \gamma\sqrt{2x-1}$, $a = \frac{d}{2}, d =$
diameter of the bar

$$\phi(ha) = (ha)\frac{J_0(ha)}{J_1(ha)}, \quad \phi(ka) = (ka)\frac{J_0(ka)}{J_1(ka)}$$

J_0
is the Bessel function of the first kind of order zero,

$$J_0(x) = \sum_{m=0}^{\infty} \frac{(-1)^m x^{2m}}{2^{2m}(m!)^2}$$

J_1
is the Bessel function of the first kind of order one,

$$J_1(x) = \sum_{m=0}^{\infty} \frac{(-1)^m x^{2m+1}}{2^{2m+1} m!\,(m+1)!}$$

The method for determining the Pochhammer-Chree modes is as follows:

1. Choose a value for the Poisson's ratio v and γa, see Figure 3.
2. Find the value of x that will give the first zero for Equation l. This is achieved by choosing values for $\frac{C_p}{C_0}$ until equation 1 is satisfied. The first zero crossing is the 1st Pochhammer-Chree mode. Subsequent zero crossings provide the higher modes.
3. Note that the first choice of $\frac{C_p}{C_0}$ is important, it is therefore recommended that the first choice of γa be almost zero and use $\frac{C_p}{C_0} = 1$, then the next choice of x can be determined form the previous value of x.

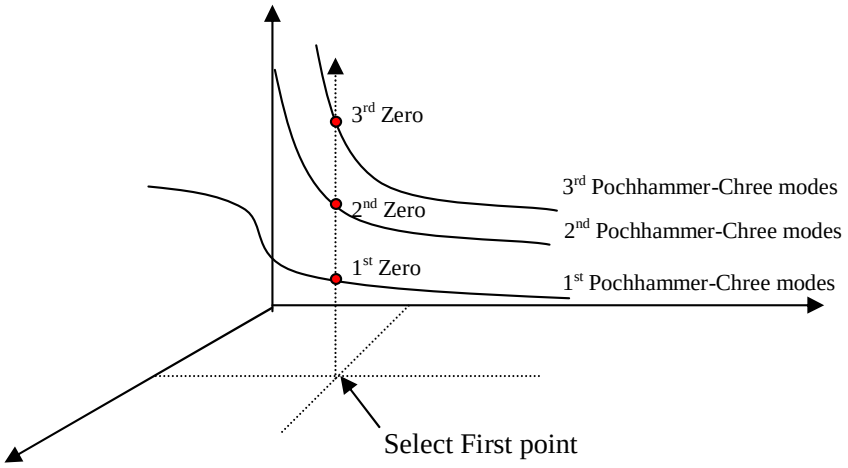

Figure 3: Graph showing the method of determining the Pochhammer-Chree modes.

The Pochhammer-Chree solution of the first mode of vibration is shown in Figure 3 for a material with a Poisson's ratio of 0.3. The graph has been normalised by dividing

the phase velocity C_p by the fundamental velocity Co, where $C_0 = \sqrt{E/\rho}$. From Figure 4 it is evident that the propagation velocity decreases with decreasing wavelength, that is a hi g h frequency wave travels slower than a lower frequency wave.

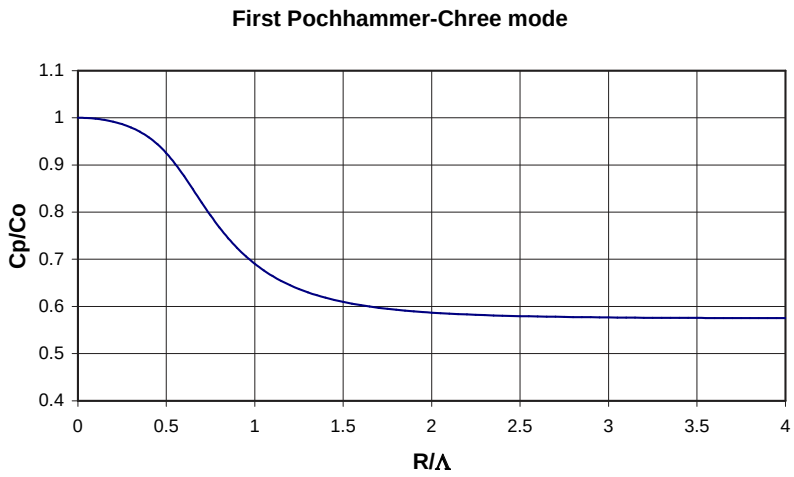

Figure 4: Solution of the dispersion equation for the first mode, showing the change in phase velocity $C_P$with wavelength Λ for a material with a Poisson's ratio of 0.3.

2.3 Correcting for Dispersion using the Fast Fourier Transform

2.3.1 Fourier Theory

To explain how dispersion correction was achieved using the FFT first some Fourier notation and concepts are necessary. Only the essential concepts are given as the details are lengthy and beyond the scope of this paper. The reader is referred elsewhere [18] for more details.

The expression

$$f(t) \Leftrightarrow F(\varpi)$$

states that the Fourier transform of the function $f(t)$from the time domain into the frequency domain is $F(\varpi)$ and the inverse Fourier transform of $F(\varpi)$ is f (t).

This moving a pulse from one point in time to another point in time the Time Shift Theorem is used, ie

$$\text{Let } f(t) \Leftrightarrow F(\varpi).$$
$$\text{Then } f(t-\tau) \Leftrightarrow F(\varpi)\, e^{-j\varpi\tau}$$

This states that when a function $f(t)$ undergoes a time shift and becomes $f(t-\tau)$, the associated Fourier transform is multiplied by a complex exponential $e^{-j\varpi\tau}$ [18].

To shift and correct for dispersion the recorded pulsed is first transformed into the frequency domain using the FFT. Then the individual frequency components are multiplied by $e^{-j\varpi\tau}$.

Where

ω = radial frequency in rad/sec of the particular frequency component under consideration.

$\tau = \mathrm{Z}/\mathrm{C}_p$ in seconds

Z is the distance to move the pulse in meters

Cp = Phase velocity, of the particular frequency component under consideration, from the Pochhammer-Chree solution.

The inverse FFT is performed and the corrected pulse is plotted.

2.4 Material Models

Models representing the behaviour of materials at high strain rate have been extensively used in finite-element simulations. For any of these models the desirable feature would be to be able to characterise the material with a limited number of laboratory tests so that the simulations could be used with more confidence. Two of these models are discussed below, these being the Cowper-Symonds [12] and Johnson-Cook model [11]. These two models were selected as they are well established in the literature and used extensively in many of the finite-element computer programmes [1]. The constitutive constants used in the model are, however, not always available for the specific material under consideration especially as a function of its microstructure and degree of cold working or work hardening.

2.4.1 Cowper-Symonds Constitutive Equation

In 1957 Cowper and Symonds introduced their constitutive equation (Equation 2) [12] to characterise the effect of strain rate on material properties. Their model was formulated by gathering test data of the dynamic lower yield stress of various materials at different strain rates. From the data a best-fit curve was generated and constitutive constants for Equation 2 were generated. From the material coefficients (D and q) the stress-strain curve of a material at a known strain rate could be scaled to determine the material properties at an unknown strain rate.

$$\frac{\sigma_0'}{\sigma_0} = 1 + \left(\frac{\dot{\varepsilon}}{D}\right)^{\frac{1}{q}} \tag{2}$$

where

σ_0' was the dynamic flow stress at a uniaxial plastic strain rate $\dot{\varepsilon}$.

σ_0 was the conceptual "static" flow stress ($\dot{\varepsilon} = 0\mathrm{s}^{-}$') inferred from experimental data.

D and q were constants for a particular material.

2.4.2 Johnson-Cook Constitutive Equation

The Johnson-Cook model was introduced in 1983 [11] and was primarily intended for computational work. The model was formulated by gathering test data at different strain rates and temperatures for a wide range of test procedures.

From these tests the model was expressed as

$$\sigma = [A + B\varepsilon^n] \cdot [1 + C \ln \dot{\varepsilon}^*] \cdot [1 - T^{*m}] \tag{3}$$

where

- ε is the equivalent plastic strain, $\dot{\varepsilon}$ is the strain rate, $\dot{\varepsilon}^* = \dot{\varepsilon}/\dot{\varepsilon}_0$ is the dimensionless plastic strain rate for $\dot{\varepsilon}_0 = 1.0s^{-1}$.
- T^* was the homologous temperature $\left(T^* = \frac{T - T_{ROOM}}{T_{MELT} - T_{ROOM}}\right)$
- A is the yield stress
- B and n represent the effects of strain hardening
- C is the strain rate constant
- m is the thermal softening fraction

These models are used, as appropriate, in the comparison of the experimental results discussed in Section 4.

3 Experimental Facility

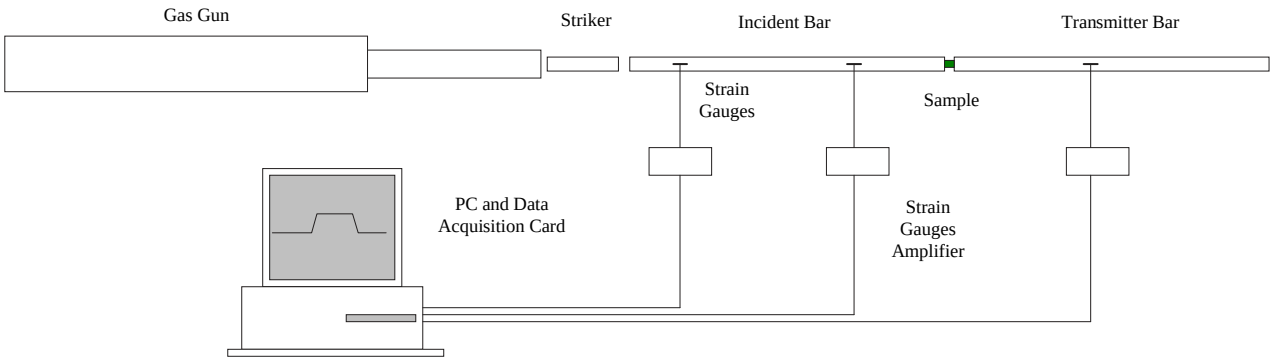

Figure 5: A Schematic representation of the split Hopkinson pressure bar used for high strain rate material testing.

The operation of the SHPB for a compression test is discussed below. The schematic layout of the system is given in Figure 5 and a photograph of the layout laboratory is Figure 6. A gas gun launches a striker bar that impacts upon the end of the incident bar. A stress wave is generated that travels down the bar and is recorded sequentially by the first and second strain gauges mounted longitudinally on the bar. The stress wave then passes through the specimen and the specimen is compressed. Part of the stress wave is reflected in the form of a tensile pulse and is recorded by the second strain gauge. Part of the wave energy is absorbed by the specimen and the remainder is transmitted to the transmitter bar and recorded by the third strain gauge mounted on the transmitter bar. The three readings are used to determine the time dependent stress state of the specimen. From the time dependent strain state data, a stress vs. strain plot can be obtained [20].



Figure 6: Photograph of the SHPB system.

The measurement of the stress wave was by means of 2mm strain gauges that were wired in a full bridge arrangement that compensates for bending and temperature. The signal from the full bridge was fed into a Burr-Brown INAl10 fast settling instrumentation amplifier, which was mounted on custom built boards, with an amplification of 1000. The signal was then fed into an ADLINKPCI-9812 high-speed data acquisition card where it was sampled, at a maximum rate of 20MHz and at 12-bit resolution, and stored as a TXT file. The data that was captured by the digital oscilloscope was fed into Excel. With an Excel-Matlab link the data was sent to Matlab, where dispersion correction was performed and then sent back to Excel. This approach

combined the use of the powerful function available in Matlab and the ease of the Excel spread sheet environment.

4 Results and Discussion

To test the dispersion correction the reading obtained from the first strain gauge station was moved to the second station without correcting for dispersion and is shown in Figure 7a. As can be seen the correlation between the two readings were not exactly coincident. The dispersion Correction was then applied, and as can be seen in Figure 7b, the correlation was far better, thus indicating that the dispersion correction was functioning correctly.

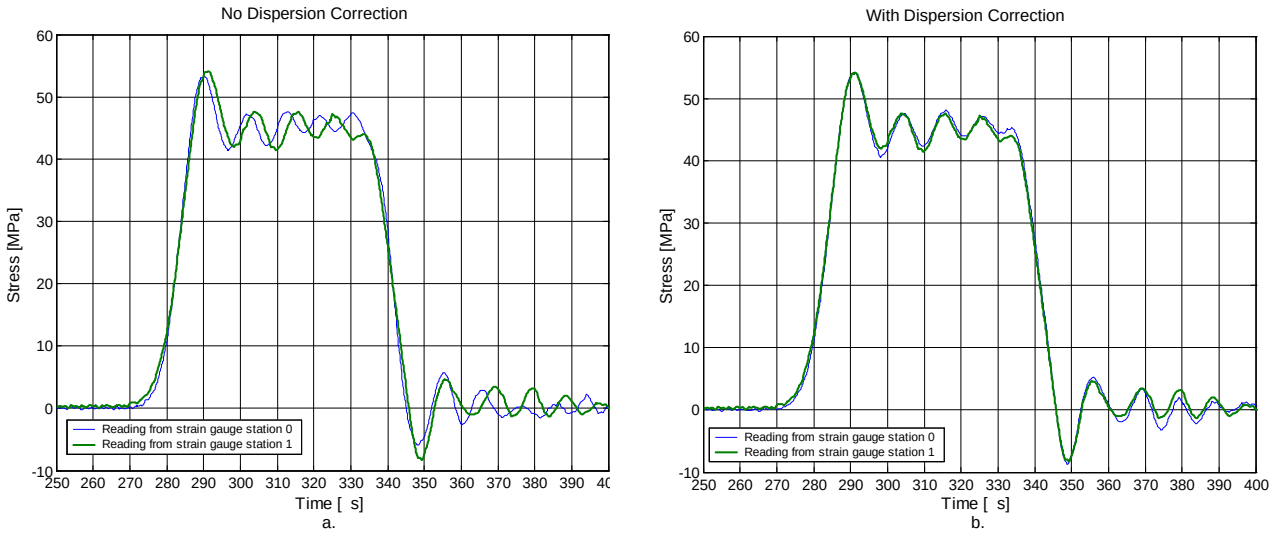

Figure 7: Comparison of data to show the effects of data that has and has not been corrected for dispersion.

Once the SHPB system was calibrated material testing could be performed. Two materials were tested namely mild steel (EN1A), and copper, in both the as-received condition as well as simply annealed copper. A typical reading of the three pulses obtained during a copper test are shown in Figure 8a. These three readings were then processed to yield the stress-strain and strain rate curves, which are shown in Figure 8b.

4.1 Comparison between the Test Data with that of Published Results and the Cowper-Symonds Model for Mild Steel

The mild steel tests were compared using the Cowper-Symonds constitutive model. This model was selected as there were published constitutive constants available for mild steel. A plot of the dynamic compression test data and the quasi-static tensile test data is given in Figure 9. The

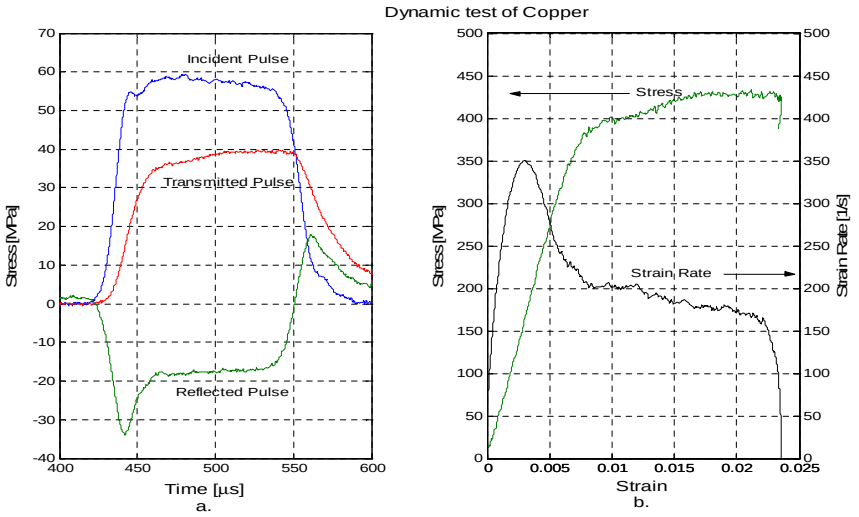

Figure 8: Copper test showing a.) Stress reading in the bar and b.) Stress-strain and strain rate plot.

mild steel dynamic test with strain rates of $360s^{-1}$ and $919s^{-1}$, and the tensile test (strain rate = $0.001s^{-1}$) were scaled using various constitutive constants for Equation 2 to a reference strain rate of $1x10^{-4}s^{-1}$ and plotted. By scaling the test data to this reference strain rate, the model could be tested as the lower yield point of the quasi-static and dynamic tests should correlate.

The first case considered dynamic uni-axial tests having small strains in the neighbourhood of the yield strain with constitutive constants of D=$40.4s^{-1}$ and q=5 [12]. The next case utilised constants obtained from Abramowicz [2] with constitutive constants of D=$802s^{-1}$ and q=3.585. These constants were determined from more recent dynamic uniaxial tensile experiments performed at the Department of Mechanical Engineering at the University of Liverpool. The last case utilised calculated values from the present test data, with the constitutive constants being determined to be D=$844s^{-1}$ and q=2.207.

From Figure 9 it can be seen that the first set of scaled curves are far from the test data curves indicating that the constitutive constants do not correlate well. The second and third sets of scaled lines are positioned effectively on top of one another, as the constitutive constants are very similar. For the second and third sets the upper yield point of the scaled quasi-static tensile test lies between the scaled dynamic compression tests, but then deviates as it moves away from the yield point. The lower yield points of the quasi-static and dynamic scaled test results do not correlate exactly but are reasonably close. The deviation is not substantial and are regarded as sufficiently correlating. In order to adjust the lower yield points to coincide the values of D=$2000s^{-1}$ and q=5 had to be used.

The mild steel test data was then compared to experimental data generated by Tanimura [19]. The data that Tanimura presented was for an annealed mild steel test at strain rates of $0.001s^{-1}$

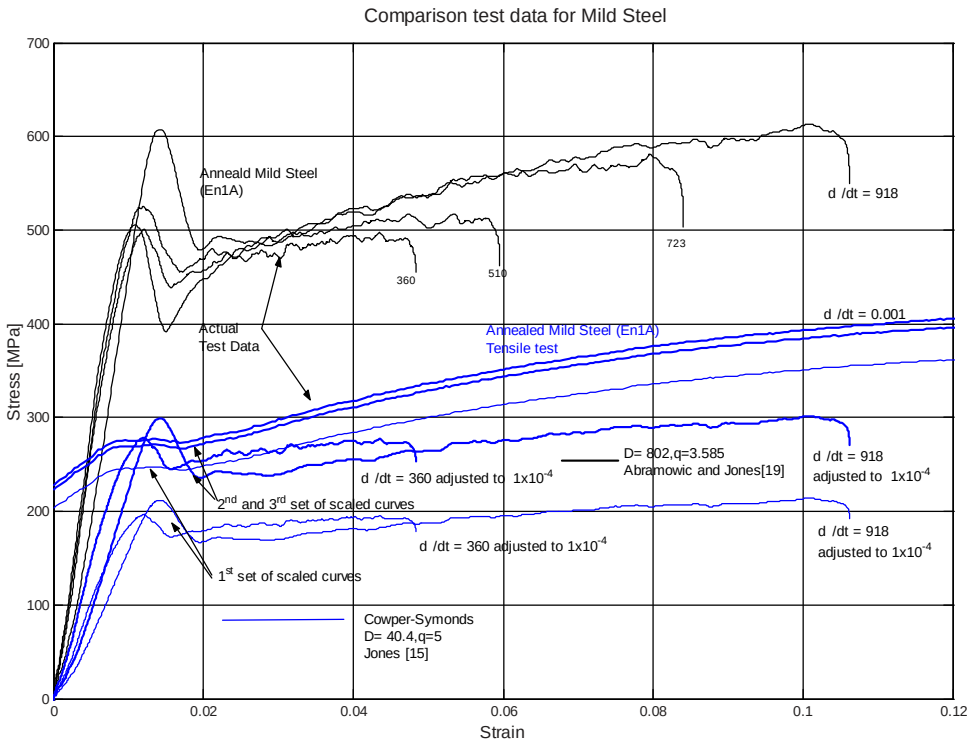

Figure 9: Comparison test data to the Cowper-Symonds constitutive model for mild steel (EN 1A). Note that the solid lines refer to the present experimental work, with the dashed lines representing the same data suitably scaled with the appropriate Cowper-Symonds coefficients taken from literature.

and 2000s^{-1}. Selected points from the Tanimura curve were plotted over the mild steel test data and are shown in Figure 10.From Figure 10 it can be seen that there is very good correlation between the quasi-static and dynamic test data. The strain rate of the Tanimura curve is higher than that of the test data and this is reflected in the upper yield point being higher than that of the curve at a strain rate of 918s^{-1}. The curve after the lower yield point correlated well except for the slight oscillation of the curve of Tanimura. These oscillations could result from the lack of dispersion correction being applied to the captured data from the pressure bars.

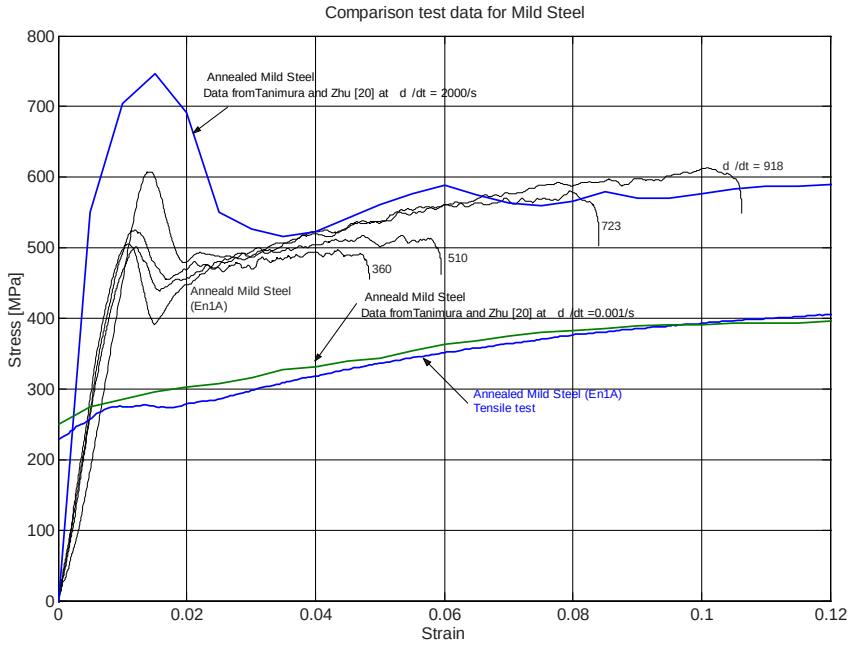

Figure 10: Comparison test data to the data obtained from Tanimura [19] for mild steel.

4.2 Comparison between the Test Data and the Johnson-Cook Model for Copper

The high strain rate tests on copper test were compared to the Johnson-Cook constitutive model [11], as there were published constitutive constants available for copper. The constitutive constants used in Equation 3 were A=90MPa, B=292MPa, n=0.31, C=0.025 and m=1.09 as taken from Johnson and Cook [11].

Figure 11 shows the dynamic compression test data as well as the quasi-static tensile test data for copper. Also plotted is the Johnson-Cook constitutive model for strain rates of 308s^{-1} and 1160s^{-1}. In Figure 11 it can be seen that the Johnson-Cook model deviates substantially at low strains, from the annealed dynamic compression test data, but at the higher strains there is closer convergence between the two traces. It can also be seen that the degree of strain rate sensitivity for the dynamic compression test and the Johnson-Cook model are quite similar.

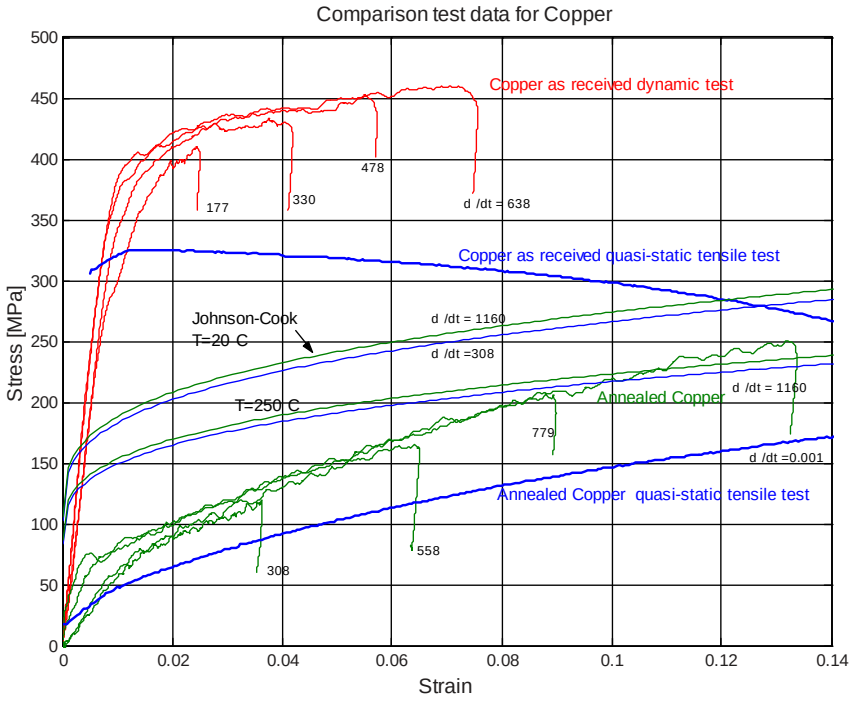

Figure 11: Comparison test data for Copper using the Johnson-Cook model.

The annealing conditions could also have resulted in the stress level being lower. The annealing utilised for specimens of size ϕ 4 x 3mm long, entailed being held at 450 $^\circ$C, for 10 minutes, and allowed to cool in the oven. In Figure 11 it can be seen that the Johnson-Cook model lies between that of the as received and annealed test results indicating that if the specimens had been only partially cold worked the stress level would probably have been higher.

The annealed quasi-static and dynamic test data was compared to published results. Firstly dynamic test data was compared to published dynamic test data, at a strain rate of 451s^{-1} by Zerilli [22]. The points published by Zerilli were plotted over the dynamic test data and are shown in Figure 12.In Figure 12 is can be seen that the published curve shows close correlation with the test data. The next published results were generated by Follansbee [7]. The quasi-static results were compared and it can seen that the published stress strain curve by Follansbee is marginally higher and is shown in Figure [3].The dynamic test stress strain curve published by Follansbee, at a strain rate of 1800s^{-1} was slightly lower than the test data but had a similar trend. The deviation between the test data and the published data was considered acceptable. The deviation could be the result of different elemental impurities composition as well as the annealing conditions as Follansbee annealed at 600 $^\circ$C in a vacuum for 60 minutes compared to the present test specimens which were annealed at 450 $^\circ$C for only 10 minutes.

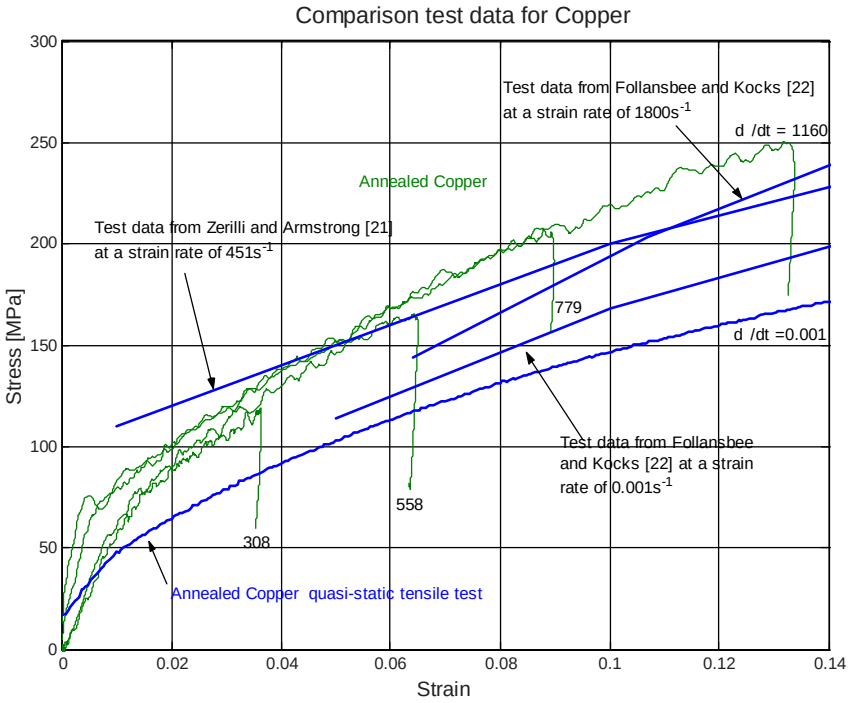

Figure 12: Comparison of annealed copper test data with published results.

5 Concluding Remarks

A data capturing and processing system has been developed which is accurate for the purposes required. The Johnson-Cook and Cowper-Symonds material models published in the literature did not correlate well with the present actual test data, when using conventional constitutive equation constants. The correlation was much improved, however, if values were used from other published results, and it is believed there are two main reasons for this. Firstly, the material tests conducted showed that there is a large difference in the stress level of an as-worked specimen compared to one that was annealed. Thus, the work hardening state and microstructure of the specimen could be the source on the discrepancy. Secondly, the value used for the constitutive constants in the model significantly altered the predicted stress level. As a result, the selection of the correct values for the constitutive constants is vital, if one is to obtain good correlation with the models.

References

[1] Karlsson 171 Hibbitt and Sorensen Inc. Abaqus theory manual version 5.8. Int. Symp. Ballistics, the Hague Netherlands, 1998.

[2] W. Abramowicz and N. Jones. Dynamic progressive buckling of circular and square tubes. Int. J. Impact Engng, 4:243–270, 1986.

[3] J.D. Achunbach. Wave Propagation in Elastic Solids, volume 16. North-Holland Pub-listing Company, 1973.

[4] D. Bancroft. The velocity of longitudinal waves in cylindrical bars. Physical Review, 1941.

[5] R.N.L. Davies. A critical study of the hopkinson pressure bar. Phil. Trans. Roy. Soc. Lond., 240:375–457, 1948.

[6] P.S. Follansbee and C. Frantz. Wave propagation in the split hopkinson pressure bar. J. Eng. Mat and Tech, 105:61–66, 1983.

[7] P.S. Follansbee and U. F. Kocks. A constitutive description of the deformation of copper based on the use of the mechanical threshold stress as an internal state variable. Acta Metall, 36:81–93, 1988.

[8] D.A. Gorham. A numerical method for the correction of dispersion in pressure bar signals. J. Phys. E: Sci.Instrum., 16:477–479, 1983.

[9] B.F.R.S. Hopkinson. A method of measuring the pressure produced in the detonation of explosives or by the impact of bullets. Phil. Trans. Roy. Soc. Lond., 213:137–456, 1914.

[10] D.Y. Hsieh and H. Kolsky. An experimental study of pulse propagation in elastic cylinders. Proc. Phys. Soc., 71, 1958.

[11] R.G. Johnson and W. H. Cook. A constitutive model and data for metals subjected to large strains, high strain rates and high temperatures. Int. Symp. Ballistics, the Hague Netherlands, 7:541–547, 1983.

[12] N. Jones. Structural Impact. Cambridge University Press, 1989.

[13] H. Kolsky. An investigation of themechanical properties of materials at very high rates of load. Proc. R. Soc. Lond., 1362:676–700, 1949.

[14] C.K.B Lee and R.C. Crawford. A new method for analysing dispersed bar gauge data. Meas. Sci. Technol., 4:931–937, 1993.

[15] C.K.B Lee and R.C. Crawford. Evidence of higher pochhammer-chree modes in an unsplit hopkinson bar. Meas. Sci. Technol., 6:853–859, 1995.

[16] J.Vl. Lipshitz and H. Leber. Data processing in the split hopkinson pressure bar test. 1nt.J.Impact, 15(6):723–733, 1994.

[17] A.E.H. Love. A Treatise on the Mathematical Theory of Elasticity. Dover, 1944.

[18] N. Morrison. Introduction to Fourier Analysis. Wiley Interscience, 1994.

[19] K. Mimura Tanimura S. and W. Zhu. A dynamic constitutive equation and its experimental verification. J.Phys. IV France, 10:33–38, 2000.

[20] M.M. Al-Mousawi S.R. Reid and W.F. Deans. The use of the split hopkinson pressure bar techniques in high strain rate materials testing. J.Mech.Eng.Sci., 221:273–292, 1997.

[21] E.H. Yew and C.S. Chen. Experimental study of dispersive waves in beams and rods using fft. J.Appl.Mech., 45:940–942, 1978.

[22] F.J. Zerilli and R. Armstrong. Dislocation-mechanics-based constitutive relations for material dynamics calculations. J. Appl. Phys., 61:1816–1825, March 1987.